lower mantle be more viscous than the upper mantle in order to produce the required positive geoid anomalies. This has already been shown to be true for the Earth, where the observed geoid highs over regions of mantle upwelling and regions of mantle downwelling are best explained by the presence of a strong lower mantle [11,12]. The large positive GTRs and the presence of large shield volcanos in certain highland regions on Venus, such as Beta Regio and Eistla Regio, are best explained as areas of mantle upwelling [5,13,14]. The regime of rapid crustal flow predicts crustal thinning over the upwelling. However, the extensive partial melt and ensuing volcanism expected over such regions of mantle may outweigh the effects of crustal thinning on the surface topography and thus also yield postive GTRs [15].

References: [1] Solomon S. C. et al. (1991) *Science, 252*, 297. [2] Kiefer W. S. et al. (1986) *GRL, 13*, 14. [3] Bills B. G. et al. (1987) *JGR, 92*, 10. [4] Phillips R. J. et al. (1991) *Science, 252*, 651. [5] Smrekar S. E. and Phillips R. J. (1991) *EPSL, 107*, 587. [6] Phillips R. J. (1986) *GRL, 13*, 1141. [7] Phillips R. J. (1990) *JGR, 95*, 1301. [8] King S. D. et al. (1990) *PEPI, 59*, 195. [9] Bindschadler D. L. and Parmentier E. M. (1990) *JGR, 95*, 21. [10] Schmeling H. and Marquart G. (1990) *GRL, 17*, 2417. [11] Richards M. A. and Hager B. H. (1984) *JGR, 89*, 5987. [12] Hager B. H. (1984) *JGR, 89*, 6003. [13] Grimm R. E. and Phillips R. J. (1991) *JGR, 96*, 8305. [14] Grimm R. E. and Phillips R. J. (1991) *JGR*, in press. [15] Phillips R. J. et al. (1991) *Science, 252*, 651.

N93-14377

VENUS GRAVITY: SUMMARY AND COMING EVENTS.

W. L. Sjogren, Jet Propulsion Laboratory, 4800 Oak Grove Drive, Pasadena CA 91109, USA.

The first significant dataset to provide local measures of venusian gravity field variations was that acquired from the Pioneer Venus Orbiter (PVO) during the 1979–1981 period. These observations were S-band Doppler radio signals from the orbiting spacecraft received at Earth-based tracking stations. Early reductions of these data were performed using two quite different techniques. Estimates of the classical spherical harmonics were made to various degrees and orders up to 10 [1,2,3]. At that time, solutions of much higher degree and order were very difficult due to computer limitations. These reductions, because of low degree and order, revealed only the most prominent features with poor spatial resolution and very reduced peak amplitudes.

Another reduction technique was the line-of-sight acceleration mapping that had been used successfully for the Moon and Mars. This approach provided much more detail and revealed the high correlation of gravity with topography [4,5,6]. However, this technique does not produce a global field as do the spherical harmonics. It provided a mapping of features from approximately 50°N to 25°S latitude for 360° of longitude. Other shortcomings were that the accelerations were at spacecraft altitude rather than at the surface and were not vertical accelerations; however, the reductions were quick and cheaply accomplished. Other efforts to analyze these data included local area reductions, where surface masses were estimated [7,8,9].

The computer revolution over the past 10 years has allowed new reductions with spherical harmonics. New fields up to degree and order fifty (2600 parameters) have been made [10,11,12]. These fields now provide the best representation for any serious geophysicist doing quantitative modeling. There is now vertical gravity at the surface from a global model that carries all the requirements of dynamical consistency. There is one sizeable concern in that the resolution over the entire planet is not uniform. This is due to the Pioneer orbit, which had a high eccentricity, causing the high latitude regions of Venus to be poorly resolved.

The Magellan (MGN) spacecraft, which went into orbit about Venus in August 1990, has returned Doppler data for gravity field reduction. However, because the high gain antenna was pointed at Venus for SAR mapping, no gravity data were acquired until the antenna was pointed back to Earth. This occurred at spacecraft altitudes higher than 2500 km, greatly reducing local gravity sensitivity. MGN has an eccentricity much smaller than PVO, so there is new information in the polar regions. Present reductions include two MGN circulations (486 days), which reduce uncertainties and produce somewhat better resolution.

During March, April, and May 1992 new low-altitude data have been acquired from both PVO and MGN. PVO periapsis latitude has changed 27°, from 16°N to 11°S. These data will provide better definition in the southern hemisphere, particularly over Artemis. The MGN mission now acquires periapsis gravity data for one orbit out of eight (i.e., foregoes SAR mapping for one orbit/day). Since MGN has an X-band radio signal, the data quality is a factor of 10 better than PVO. Only a small block of MGN data was acquired before its periapsis went into occultation May 16. Solar conjunction and periapsis occultation has also occurred for PVO.

In September of 1992 MGN periapsis will exit occultation and its periapsis altitude will be lowered to approximately 170 km. Periapsis will be visible from Earth for a complete 360° longitude coverage period (243 days). This should be an excellent dataset, having low X-band data noise that in turn can be combined with the PVO dataset.

In December 1992 PVO will exit periapsis occultation and low-altitude data (~150 km) in the southern hemisphere will be acquired for about one month before PVO is lost due to the lack of fuel to maneuver to safe altitudes.

In May 1993 there remains the possibility of aerobraking MGN into a circular orbit, thus allowing global uniform resolution gravity data to be acquired. One hopes that NASA has enough foresight to keep Magellan alive so this is a reality. It is anticipated that if this is done, harmonic solutions to degree and order 60–70 (5000 parameters) will be produced. One could then compare similar features globally, resolve coronae and test many interior structure models.

References: [1] Ananda M. P. et al. (1980) *JGR, 85*, 8303–8318. [2] Williams B. G. et al. (1982) *Icarus, 56*, 578–589. [3] Mottinger N. A. et al. (1985) *Proc. LPSC 15th*, in *JGR, 90*, C739–C756. [4] Phillips R. J. et al. (1979) *Science, 205*, 93–96. [5] Sjogren W. L. et al. (1980) *JGR, 85*, 8295–8302. [6] Sjogren W. L. et al. (1983) *JGR, 88*, 1119–1128. [7] Esposito P. B. et al. (1982) *Icarus, 51*, 448–459. [8] Reasenberg R. D. et al. (1981) *JGR, 86*, 7173–7199. [9] Sjogren W. L. et al. (1984) *GRL, 11*, 489–491. [10] Nerem R. S. (1991) *Eos, 72*, 174–175. [11] McNamee J. B. et al. (1992) *JGR*, in press. [12] Konopliv A. R. (1992) private communication of results to be published (AGU presentation in Montreal, Canada).

N93-14378

DIFFERENT TYPES OF SMALL VOLCANOS ON VENUS.

E. N. Slyuta[1], I. V. Shalimov[2], and A. M. Nikishin[2], [1]Vernadsky Institute, Russian Academy of Science, 117975 Moscow, Russia, [2]Moscow University, Moscow, Russia.

One of the studies of volcanic activity on Venus is the comparison of that with the analogous volcanic activity on Earth. The preliminary report of such a comparison and description of a small

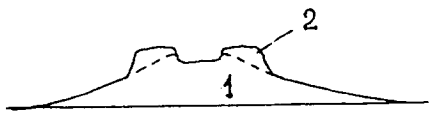

Fig. 1. Sketchy cross-section of flat-top volcanos: 1–shield edifice; 2–cinder flat-top superstructure.

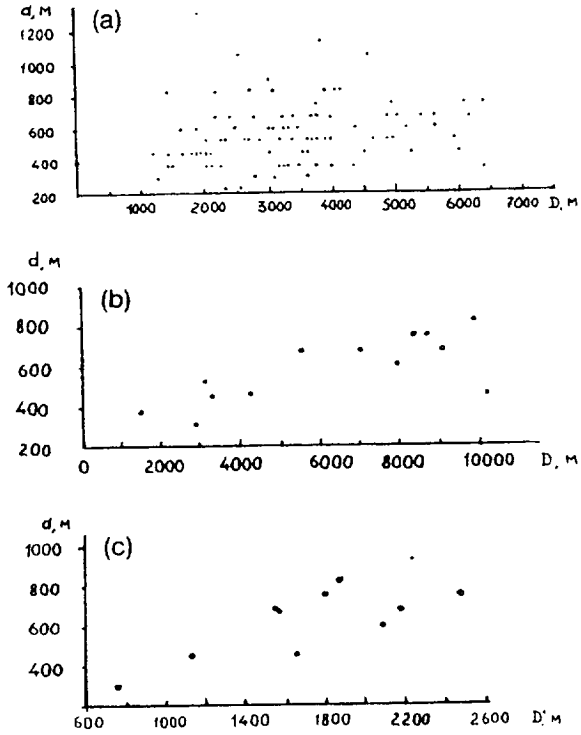

Fig. 2. Distribution of pit diameters relative to edifice diameters: (a) usual small shields; (b) flat-top volcanos (pit diameter relative to shield diameter); (c) flat-top volcanos (pit diameter relative to flat-top part diameter).

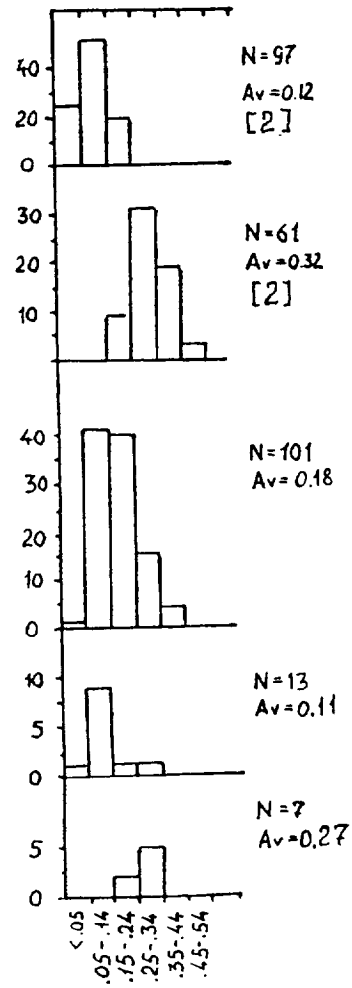

Fig. 3. Comparison of crater/edifice diameter ratio histograms for small venusian volcanos (bottom) and possible terrestrial analogs.

cluster of small venusian volcanos is represented in detail in this paper.

The cluster in question of small volcanos on Venus within Sedna Planitia (43°N, 334°E) is localized and compact. The total number of small volcanos recognized within the cluster is about 160 edifices; most of them have a small top pit. Some types of volcanic edifices within the cluster are recognized. The major type of volcanic edifices is small shield volcanos of Iceland type [1]. Small shield average basal diameter is 3750 m. Volcanos with a flat top outlined by a steep flank (Fig. 1) are also observed. There are 15 flat-top edifices (~ 9, 4% of the total number) in the cluster. The basal diameter of those varies from 1500 m to 10,200 m and average basal diameter is 6450 m, i.e., they are sufficiently larger on the average than usual shield edifices. Another difference from regular small shield volcanos is the dependence observed between the crater diameter and the edifice diameter (Figs. 2a,b). The right dependence between crater diameter and flat-top edifice diameter is also observed (Fig. 2c). The crater diameter to edifice basal diameter ratio is similar to that for shield edifices and terrestrial small shields (Fig. 3) [2]. The crater diameter to flat-top part basal diameter is similar to that for terrestrial cinder cones (Fig. 3). If the slope angle of the flat-top flank corresponds to the angle of natural slip (of rest) of volcanic cinder material on Earth (it is about 30° [3]) the flat-top height can be defined, which varies from 130 to 260 m for different size edifices.

Thus, at least there are two different morphological types of small volcanos within the cluster. The difference may be caused by both eruption conditions including volatile content and different magma compound. It is suggested that venusian flat-top volcanos may have formed in two stages. The first is the formation of usual shield edifice due to effusive eruption and the second is the formation of the flat cinder superstructure on the shield top (Fig. 1) due to subsequently more explosive eruption.

It should be emphasized that venusian small shields are also similar to terrestrial analogs in size [1]. The minimal basal diameter of a venusian small shield obtained by more than 600 measure-

ments of volcanos with accuracy down to pixel is within the 800–900-m range. The smallest terrestrial shield edifice formed by one eruption also has a basal diameter of about 800–900 m [3].

The different types of volcanos can often be observed within the similar volcanic cluster on Earth. There are a variety of volcanic structures in similar clusters of volcanos in Saudi Arabia. The volcanic cluster and volcanos have been described in detail by Camp and Roobol [4]. The scoria cones are 0.5 to 1.3 km in diameter and rise as much as 100 m above the surrounding surface. They are typically steep and have open craters with a diameter of 100–400 m. Scoria cones are the largest group of Arabian volcanos with numbers up to 75% [4]. The shield volcanos are 5–10 km in diameter and rise as much as 1150 m above the surrounding surface. The crater/cone ratio is smaller, which is typical for shield volcanos. This group reaches 12% of the total number of volcanos [4].

References: [1] Sinilo V. P. and Slyuta E. N. (1989) *LPSC XX*, 1016–1017. [2] Frey H. and Jarosewich M. (1982) *JGR*, *87*, 9867–9879. [3] Macdonald G. A. (1972) *Volcanoes*, Prentice-Hall, New Jersey. [4] Camp V. E. et al. (1991) *GSA Bull.*, *103*, 363–391.

N93-14379

CONSTRAINTS ON CRUSTAL RHEOLOGY AND AGE OF DEFORMATION FROM MODELS OF GRAVITATIONAL SPREADING IN ISHTAR TERRA, VENUS. Suzanne E. Smrekar and Sean C. Solomon, Department of Earth, Atmospheric, and Planetary Sciences, Massachusetts Institute of Technology, Cambridge MA 02139, USA.

Introduction: Gravitational spreading is expected to lead to rapid relaxation of high relief due to the high surface temperature and associated weak crust on Venus [1,2]. In this study, we use new Magellan radar and altimetry data to determine the extent of gravitational relaxation in Ishtar Terra, which contains the highest relief on Venus as well as areas of extremely high topographic slope. Within Ishtar Terra the only mountain belts found on Venus, Akna, Danu, Freyja, and Maxwell Montes, nearly encircle the smooth, high (3–4 km) plateau of Lakshmi Planum. Finite-element models of this process give expected timescales for relaxation of relief and failure at the surface. From these modeling results we attempt to constrain the strength of the crust and timescales of deformation in Ishtar Terra. Below we discuss observational evidence for gravitational spreading in Ishtar Terra, results from the finite-element modeling, independent age constraints, and implications for the rheology and timing of deformation.

Observations: Magellan data have revealed abundant evidence for localized extension throughout Ishtar Terra [3,4]. Many of the observed extensional features are oriented perpendicular to the downslope direction, implying that they formed as a result of gravitational spreading. In some of the mountainous areas, extensional faults occur parallel to the apparent direction of shortening. By analogy with the Himalayas on Earth [5], we interpret such extension to indicate gravitational spreading during convergence. Areas of possible gravitational spreading are observed in each of the four mountain belts and along both the southern and northeastern margins of Lakshmi Planum. Horizontal strain in these regions is estimated to be 1–20%; this value may be an underestimate if blocks are rotated along the normal faults. The observational evidence for gravitational spreading in Ishtar Terra is discussed more fully in [4].

Models: We use the finite-element algorithm TECTON [6] to model the evolution of gravitational spreading in a vertical section of the crust near the margin of a plateau or the edge of a broad mountain belt. Each model includes an elevated plateau 50 km in width, a sloped margin, and a lowlands region 80 km in width. The code employs a depth-dependent, viscoelastic rheology with nonlinear stress dependence and exponential temperature dependence. We adopt a Young's modulus of 6×10^{10} Pa, a Poisson's ratio of 0.25, and a diabase flow law [7]. Although a diabase composition is most similar to the composition determined at Soviet lander sites [8], the flow law determined for diabase may underestimate the strength because of partial melting of samples during the experiment [7,9]. For this reason, we also employ a websterite flow law [10] as an approximate upper bound on crustal strength. The surface temperature is 740 K and increases linearly with depth. Each row of elements in the grid has the same viscosity, which is equivalent to assuming that the temperature is constant along both the bottom and top of the grid. This results in a somewhat higher thermal gradient in the plains than in the plateau. The boundary conditions are zero vertical and horizontal velocity on the bottom of the grid, a free surface top boundary, and zero horizontal velocity and free vertical slip at the sides. The bottom boundary condition approximates an upper mantle layer that is much stronger than the lower crust. Details of the models are given in [4]. Brittle failure is evaluated using a Mohr-Coulomb criterion. The timing of predicted brittle failure and relaxation of relief are found for ranges of plateau height (1–5 km), plateau margin slope (1°–30°), crustal thickness (10–30 km), and thermal gradient (5–25 K/km). Slopes of 1°–30° and plateau or mountain belt heights of 1–6 km are observed in Ishtar Terra. Crustal thickness on Venus is predicted to be 10–30 km [11,12]; the average thermal gradient is expected to be 10–25 K/km [13,14].

The rate of deformation is largely controlled by the effective viscosity, and thus the temperature and stress, at the base of the crust. The greatest deformation occurs at the base of the crust, where the viscosity is lowest. Temperature at the base of the crust increases with crustal thickness (for a fixed thermal gradient), and deviatoric stress near the base of the crust increases with both crustal thickness and plateau elevation. The nonlinear change in predicted failure and relaxation time (see below) is due both to the exponential dependence on temperature and to the power law dependence on deviatoric stress of the effective viscosity.

Failure is predicted to occur when the stresses exceed the Mohr-Coulomb criterion. The earliest failure is located on the plateau. In most cases, failure on the slope follows shortly after failure on the plateau; thrust faulting in the plains is predicted typically only for a crustal thickness of 30 km. Figure 1 shows the time from the start of spreading until the first failure on the plateau as a function of plateau height and crustal thickness, for a margin slope of 3° and a thermal gradient of 15 K/km. Models with both websterite and diabase flow laws are plotted. No times are shown for models that do not fail within 1 Ga. Cases with a diabase rheology, a large plateau height, and a large crustal thickness fail almost immediately. A plateau height of 1 km and a crustal thicknesses of 10 km can take up to tens of millions of years to fail. With a websterite flow law, no failure occurs unless the crust is a least 20 km thick and the plateau elevation is 1–3 km. Changing the thermal gradient by 10 K/km has a large effect on failure times, with a higher thermal gradient decreasing the failure time by a factor of 10^2–10^4, and a lower thermal gradient increasing times by a similar factor. When failure is first predicted, the horizontal surface strain is approximately 0.05%. This strain is unlikely to be recognized as normal faulting in Magellan radar images; a strain of 1%, which accumulates once significant relaxation of the topography begins, is probably a more reasonable value to compare with observations. As faulting is not explicitly modeled, there is some uncertainty in the interpretation of